CFAR Detection for the Complex Approximated Message Passing Reconstructed SAR Image

Hui Bi[a,b*], Bingchen Zhang[b], Xiao Xiang Zhu[c,d], Wen Hong[b], and Yirong Wu[b]

[a]*University of Chinese Academy of Sciences (UCAS). Beijing 100190, China*
[b]*Science and Technology on Microwave Imaging Laboratory,*
Institute of Electronics, Chinese Academy of Sciences (IECAS). Beijing 100190, China
[c]*Remote Sensing Technology Institute (IMF), German Aerospace Center (DLR). Oberpfaffenhofen 82234, Germany*
[d]*Signal Processing in Earth Observation (SiPEO), Technical University of Munich (TUM), 80333 Munich, Germany*
*Corresponding author. Email: bihui1991@163.com

***Abstract*—Complex approximated message passing (CAMP) is an iterative recovery algorithm for L_1 regularization reconstruction which can achieve sparse and non-sparse estimations of original signal simultaneously. This paper demonstrates a CAMP-based synthetic aperture radar (SAR) image regularization reconstruction method along with a constant false alarm rate (CFAR) detection via the output non-sparse image of CAMP iterative algorithm. Compared with iterative thresholding algorithm (ITA) and orthogonal matching pursuit (OMP), the conventional L_1 regularization reconstruction techniques, it not only can improve SAR image performance, but also its non-sparse estimation retains a similar background statistical distribution as conventional matched filtering (MF)-based techniques, which can be used for CFAR detection efficiently. Simulated and experimental results validate the effectiveness of the designed CFAR detector for the CAMP reconstructed SAR image.**

Keywords*—Synthetic aperture radar (SAR), L_1 regularization, complex approximated message passing (CAMP), constant false alarm rate (CFAR) detection.

I. Introduction

Synthetic aperture radar (SAR) is an active radar usually mounted on a moving platform, *e.g.* airplane or satellite [1]–[3]. Range Doppler (RDA) [4] and Chirp Scaling algorithms [5] are well-known matched filtering (MF)-based SAR focusing algorithms. In general, MF-based SAR imaging algorithms are computationally efficient, but the reconstructed image may have clutter and sidelobes, which restrict their application in target identification, feature extraction, *etc*. Compressive sensing (CS) [6] [7], an important development in sparse signal processing, was proposed by Donoho *et. al.* in 2006. In 2007, Baraniuk and Steeghs first demonstrated CS theory to radar imaging [8]. Inspired by this, sparse reconstruction and CS was widely used and led to promising results in radar signal processing, *e.g.*, synthetic aperture radar tomography (TomoSAR) [9] [10], inverse synthetic aperture radar (ISAR) [11], ground penetrating radar (GPR) [12], and MIMO [13]. Sparse signal processing can also be used in SAR imaging. In 2012, Zhang *et. al.* demonstrated this combination, called sparse microwave imaging, and reconstructed the surveillance region by solving a $L_q\,(0 < q \leq 1)$ regularization optimization problem, which made it possible to process the full and down-sampled raw data directly [14]. Compared to MF-based SAR imaging techniques, L_q regularization-based SAR imaging efficiently improves the image quality including reducing sidelobes and clutter. However, conventional L_q regularization methods need to transfer the two-dimensional (2D) raw data into a vector to reconstruct the surveillance region, which is time-consuming and produces significant computational complexity. Hence, is very difficult to apply to practical imaging processings.

In this paper, we present a SAR image regularization reconstruction mechanism using complex image data, and detail this mechanism from model construction, algorithm derivation to parameter setting. Compared to the regularization-based SAR imaging with full raw data, is can decreases computational cost and achieve similar reconstructed image quality. In addition, we exploit complex approximated message passing (CAMP) [15]– [17], to solve the L_1 regularization problem, due to it not only can obtain the sparse image of the considered scene as typical recovery algorithms, *e.g.* iterative thresholding (ITA) [18], but also a non-sparse estimation of the surveillance region with image statistical properties similar to the MF-based result, and hence can be used to several post-processing applications with the precondition is preserving image statistical property, *e.g.*, constant false alarm rate (CFAR) detection in this paper.

II. CAMP-based SAR Image L_1 Regularization Reconstruction

In this section, we focus on the general formalization of the imaging model, with detailed introduction of a CAMP iterative algorithm for L_1 regularization reconstruction via SAR complex image data.

A. SAR Imaging via MF

The 2D SAR imaging model can be represented as

$$\mathbf{Y} = \mathbf{H}\mathbf{X} + \mathbf{N}_0 \tag{1}$$

where $\mathbf{Y} \in \mathbb{C}^{N_a \times N_r}$ is raw data; a is azimuth time, r is range time; $\mathbf{X} \in \mathbb{C}^{N_u \times N_v}$; u is azimuth position, 2D echo data; v is ground range position, backscattered coefficient of the surveillance region; $\mathbf{H}$ is radar system observation matrix, and $\mathbf{N}_0$ is noise. Let $\mathcal{R}\,(*)$ indicate the MF-based SAR imaging

procedure, *e.g.*, RDA [4], the surveillance region $\mathbf{X}$ can be reconstructed by

$$\mathbf{X}_{MF} = \mathcal{R}(\mathbf{Y}). \tag{2}$$

MF is the typical SAR imaging method which has been widely used in the processing of SAR raw data. It can recover the considered scene accurately and computationally efficient, but the reconstructed image may suffer severely from clutter and sidelobes, which restrict their further application. To solve this problem, we propose a CAMP-based L_1 regularization SAR image reconstruction method, to achieve high-resolution reconstruction and performance improvement for existing MF-based SAR complex image.

B. Signal Model

We can express the model as

$$\mathbf{X}_{MF} = \mathbf{X}_{SP} + \mathbf{N} \tag{3}$$

where $\mathbf{X}_{SP}$ is the reconstructed SAR image from the regularization technique, and $\mathbf{N}$ is the complex matrix which denotes the difference between the MF reconstructed image and the regularization technique. $\mathbf{N}$ includes noise, clutter, sidelobes, *etc*. We can recover $\mathbf{X}_{SP}$ with known $\mathbf{X}_{MF}$ by solving the following regularization problem

$$\min_{\mathbf{X}_{SP}} \left\{ \|\mathbf{X}_{MF} - \mathbf{X}_{SP}\|_F^2 + \lambda \|\mathbf{X}_{SP}\|_q^q \right\}. \tag{4}$$

Lasso is an efficient L_1 regularization recovery method for the (3) model,

$$\hat{\mathbf{X}}_{SP} = \min_{\mathbf{X}_{SP}} \left\{ \frac{1}{2} \|\mathbf{X}_{MF} - \mathbf{X}_{SP}\|_F^2 + \lambda \|\mathbf{X}_{SP}\|_1 \right\} \tag{5}$$

where $\hat{\mathbf{X}}_{SP}$ is the iterative recovery result of $\mathbf{X}_{SP}$, and λ is the regularization parameter. The closed form solution is

$$\eta(\mathbf{X}_{MF}; \lambda) \triangleq (|\mathbf{X}_{MF}| - \lambda) e^{j \cdot \mathrm{angle}(\mathbf{X}_{MF})} \mathbf{1}(|\mathbf{X}_{MF}| > \lambda), \tag{6}$$

where $\mathbf{1}(\cdot)$ is the indicator factor, $\mathrm{angle}(\cdot)$ the complex element phase, and $\eta(\mathbf{X}_{MF}; \lambda)$ is the complex soft thresholding function applied component-wise to the input element $\mathbf{X}_{MF}$.

C. CAMP Iterative Recovery

Above L_q regularization problem in (4) can be solved efficiently by OMP, ITA, *etc*. However, these algorithms will not return an image that preserves the statistical properties of the result recovered by MF-based imaging, which restrict application of the reconstructed SAR image. CAMP [16] not only can achieve sparse reconstruction (sparse solution), but also obtain the image with similar background distribution as the MF-based recovered result. Incorporating the complex soft thresholding function $\eta(\mathbf{X}_{MF}; \lambda)$, we proposed a CAMP algorithm for the iterative reconstruction of the considered scene via Lasso model (5), as shown in Table I. Where $\tilde{\mathbf{X}}_{SP}^{(t)}$ is the non-sparse noisy estimation of the considered scene, $\mathbf{X}$, at iterative step t. $\left|\hat{\mathbf{X}}_{SP}^{(t+1)}\right|_{k+1}$ denotes the $k+1$ largest component of $\left|\hat{\mathbf{X}}_{SP}^{(t+1)}\right|$ with $k = \|\mathbf{X}\|_0$, $\langle\cdot\rangle$ is the average operator, η^R and η^I are the real and imagery part of complex soft thresholding function η, $\frac{\partial \eta^R}{\partial x_R}$ and $\frac{\partial \eta^I}{\partial x_I}$ are the partial derivative of η^R and η^I with respect to the real and imagery part of input element, respectively.

TABLE I. ITERATIVE PROCEDURE OF CAMP-BASED L_1 REGULARIZATION SAR IMAGE RECONSTRUCTION

Input:	MF-based radar complex image data $\mathbf{X}_{MF}$	
Initial:	$\hat{\mathbf{X}}_{SP}^{(0)} = \mathbf{0}$	
	$\mathbf{W}^{(0)} = \mathbf{X}_{MF}$	
	Iterative parameter τ	
	Error parameter ε	
	Maximum iterative step $T_{\max}$	
Step 1:	**While** $t \le T_{\max}$ and Residual $>\varepsilon$	
Step 2:	$\tilde{\mathbf{X}}_{SP}^{(t+1)}$	$= \mathbf{W}^{(t)} + \hat{\mathbf{X}}_{SP}^{(t)}$
Step 3:	σ_{t+1}	$= \left\|\tilde{\mathbf{X}}_{SP}^{(t+1)}\right\|_{k+1}$
Step 4:	$\mathbf{W}^{(t+1)}$	$= \mathbf{X}_{MF} - \hat{\mathbf{X}}_{SP}^{(t)} + \mathbf{W}^{(t)} \frac{1}{2}$ $\cdot \left(\left\langle \frac{\partial \eta^R}{\partial x_R} \left(\tilde{\mathbf{X}}_{SP}^{(t+1)}; \tau\sigma_{t+1} \right) \right\rangle \right.$ $+ \left. \left\langle \frac{\partial \eta^I}{\partial x_I} \left(\tilde{\mathbf{X}}_{SP}^{(t+1)}; \tau\sigma_{t+1} \right) \right\rangle \right)$
Step 5:	$\hat{\mathbf{X}}_{SP}^{(t+1)}$	$= \eta\left(\tilde{\mathbf{X}}_{SP}^{(t+1)}; \tau\sigma_{t+1} \right)$
Step 6:	Residual	$= \left\| \hat{\mathbf{X}}_{SP}^{(t+1)} - \hat{\mathbf{X}}_{SP}^{(t)} \right\|_F$
Step 7:	$t = t + 1$	
Step 8:	**end**	
Output:	Reconstructed sparse image $\hat{\mathbf{X}}_{SP} = \hat{\mathbf{X}}_{SP}^{(t+1)}$	
	Reconstructed non-sparse image $\tilde{\mathbf{X}}_{SP} = \tilde{\mathbf{X}}_{SP}^{(t+1)}$	

D. Parameter Employed

Several components of the proposed CAMP iterative algorithm are

1) $\hat{\mathbf{X}}_{SP}$ is the reconstructed sparse image with similar image performance improvement as conventional L_1 regularization SAR imaging techniques, and can achieve effective sidelobe and clutter suppression compared with MF-based SAR images.
2) $\tilde{\mathbf{X}}_{SP}$ is the reconstructed non-sparse and noisy estimation of $\mathbf{X}$. The definition of the "noise" matrix, $\mathbf{Z}^{(t)}$ following

$$\mathbf{Z}^{(t)} \triangleq \tilde{\mathbf{X}}_{SP}^{(t)} - \mathbf{X}. \tag{7}$$

3) σ_t is the standard deviation of $\mathbf{Z}^{(t)}$, and $\sigma_* = \lim_{t\to\infty} \sigma_t$ is used in the next iteration. In practical, the noise and clutter distributions are unknown, so we use $\sigma_t = \left|\tilde{\mathbf{X}}_{SP}^{(t)}\right|_{k+1}$ as an estimation of σ_t, as shown in Tables I.
4) Regularization parameter λ should be chosen to satisfy

$$0 < \lambda \le \|\mathbf{X}_{MF}\|_\infty. \tag{8}$$

5) The set of thresholding parameter τ relies on σ_* and λ. CAMP and Lasso algorithms are connected through the relationship between τ and λ. According

to [16], if τ satisfies

$$\lambda \triangleq \tau\sigma_* \left(1 - \frac{1}{2\delta}\, \mathbb{E}\left(\left\langle \frac{\partial \eta^R}{\partial x_R}\left(\tilde{\mathbf{X}}_{SP}; \tau\sigma_*\right)\right\rangle + \left\langle \frac{\partial \eta^I}{\partial x_I}\left(\tilde{\mathbf{X}}_{SP}; \tau\sigma_*\right)\right\rangle\right)\right) \tag{9}$$

then CAMP with thresholding τ can be used to solve the Lasso problem with regularization parameter λ, where $\mathbb{E}(\cdot)$ is the expectation operator. In our proposed method, we set $\sigma_* = \left|\tilde{\mathbf{X}}_{SP}\right|_{k+1}$, and $\lambda_{\max}=\|\mathbf{X}_{MF}\|_\infty$, to estimate the upper bound of τ as $\tau_{\max}$ through (9).

III. CFAR DETECTION BASED ON THE RECOVERED NON-SPARSE IMAGE OF CAMP

In 2013, Anitori *et al.* demonstrated that the gaussianity of "noise" matrix $\mathbf{Z}$ as the precondition of non-sparse output from the CAMP algorithm based CFAR detector, and verified that when the measurement matrix $\mathbf{\Phi}$, is a partial Fourier matrix which is formed by transmitting stepped frequency waveforms, *e.g.* radar application, Gaussian distribution of the real and imaginary parts is satisfied as $\mathbf{\Phi}$ is Gaussian matrix [17]. Therefore, CFAR would be effective for target detection using CAMP recovered non-sparse images in stepped frequency radar. Similar to the Gaussian measurement matrix, we have verified "noise" vector $\mathbf{Z}$ based on Chirp matrix also has Gaussianity. Thus, CFAR detection is practicable for CAMP recovered non-sparse SAR images.

CFAR detection for a ship target based on the amplitude image of the reconstructed non-sparse result via CAMP iteration is demonstrated. CFAR detection is performed for each pixel of the amplitude image in turn. The test pixel is surrounded by a target box located in a guard area, and further a background region. The guard area ensures that no pixel of an extended target is located in the background region, which would change the statistical properties of clutter and noise in the background. In the practical CFAR operation, the size of target, guard, and background windows should be adapted to the range and azimuth resolution and the target size, *e.g.* a ship in this paper [19]. For CFAR detection, the probability of false alarm P_{FA} with threshold β is

$$P_{FA} = 1 - \int_{-\infty}^{\beta} f(x)dx = \int_{\beta}^{+\infty} f(x)\,dx \tag{10}$$

where $f(x)$ is the probability density function (PDF) of the background area, *i.e.*, representing the noise and clutter distribution with pixel value x. After setting the probability of false alarm and obtaining an estimation of the background distribution, we can calculate the threshold, β, by solving (10).

We exploit the CFAR processor to perform ship detection using TerraSAR-X images being used Gaussian distribution as the approximation for the sea surface which is the clutter in ship detection [19]. With the above approximation, the CFAR detector can be expressed as

$$\left|\tilde{\mathbf{X}}_{SP}\right|_{(n_u,n_v)} \Leftrightarrow \begin{cases} \text{Target}, & if\ \left|\tilde{\mathbf{X}}_{SP}\right|_{(n_u,n_v)} > \mu_B + \sigma_B\beta \\ \text{No Target}, & else \end{cases} \tag{11}$$

where $n_u = 1, 2, \cdots, N_u$; $n_v = 1, 2, \cdots; N_v$, $\left|\tilde{\mathbf{X}}_{SP}\right|_{(n_u,n_v)}$ is the pixel under text in the amplitude image of the reconstructed non-sparse result $\tilde{\mathbf{X}}_{SP}$ via CAMP, μ_B and σ_B are the mean and standard deviation of the background area Ω,

$$\mu_B = \frac{1}{N_\Omega} \sum_{(n_u,n_v)\in\Omega} \left|\tilde{\mathbf{X}}_{SP}\right|_{(n_u,n_v)} \tag{12}$$

and

$$\sigma_B = \sqrt{\frac{1}{N_\Omega} \sum_{(n_u,n_v)\in\Omega} \left(\left|\tilde{\mathbf{X}}_{SP}\right|_{(n_u,n_v)} - \mu_B\right)^2} \tag{13}$$

respectively, where N_Ω is the number of pixels in the background area. In the CFAR detector, β is the threshold parameter which controls the probability of false alarm.

IV. EXPERIMENT AND DISCUSSION

The proposed methods were validated using several experiments with simulated and TerraSAR-X image data. To illustrate the performance improvement, let us define the target-to-background ratio (TBR) [20] to evaluate clutter suppression,

$$\mathrm{TBR}(\mathbf{X}) \triangleq 20\log_{10}\left(\frac{\max_{(u,v)\in\mathcal{T}}\left|(\mathbf{X})_{(u,v)}\right|}{(1/N_\mathcal{B})\sum_{(u,v)\in\mathcal{B}}\left|(\mathbf{X})_{(u,v)}\right|}\right) \tag{14}$$

where $\mathcal{T}$ is the target area, which is surrounded by the background region, $\mathcal{B}$ and $N_\mathcal{B}$ is the number of pixels in $\mathcal{B}$.

A. Simulated Data

Two point targets is set as the considered scene without noise and clutter to validate the effect of sidelobe suppression. Fig. 1 shows the image reconstructed by MF and our proposed method, respectively. The sparse image $\tilde{\mathbf{X}}_{SP}$ (see Fig. 1(b)) reconstructed by our proposed method completely remove sidelobes, regardless of azimuth or range direction. However, these results were obtained for the ideal condition, *i.e.*, the signal-to-clutter ratio (SCR) $= \infty$. In practical SAR imaging, we could not expect to achieve such perfect suppression. Fig. 1(c) is the reconstructed non-sparse image, $\tilde{\mathbf{X}}_{SP}$, of the considered scene via the proposed method. Comparing with Fig. 1(a) and Fig. 1(b), $\tilde{\mathbf{X}}_{SP}$ not only protrude the target as regularization-based method, but also retains the background distribution as MF-based image only with amplitude decreased approximately 50 dB. This characteristic will be very helpful in CFAR detection.

Four point targets with different amplitude, phase, and position were set as the considered scene (see Fig. 2(a)). To perform meaningful comparisons, we artificially introduced clutter to the simulated echo data of point targets, and then reconstructed the scene by MF and our proposed methods. Compared to MF, our proposed (see Fig. 2(c)) can efficiently suppress clutter and recovered the four point targets positions accurately. Quantitative analysis of clutter suppression with TBR is shown in Table II. Target1–Target4 are defined from near to far. Table II accords with the visual representation in Fig. 2, *i.e.*, the proposed algorithms can suppress clutter efficiently. Fig. 2(d) is the reconstructed non-sparse image

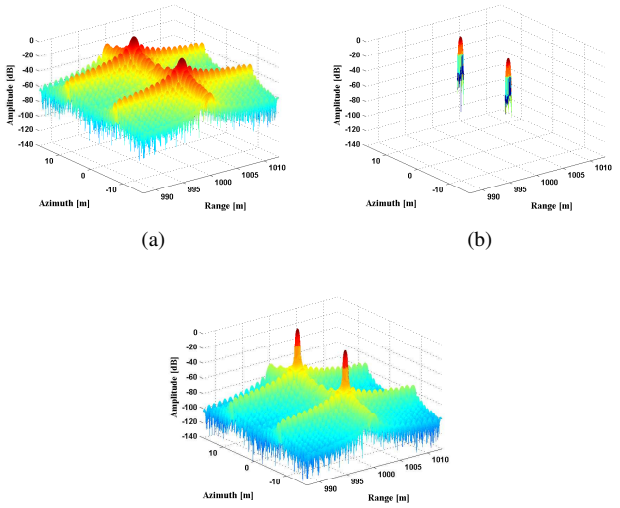

(a) (b)

(c)

Fig. 1. Reconstructed two point targets by different methods. (a) MF, (b) sparse image $\hat{\mathbf{X}}_{SP}$ reconstructed by our proposed method, and (c) non-sparse image $\tilde{\mathbf{X}}_{SP}$ reconstructed by our proposed method.

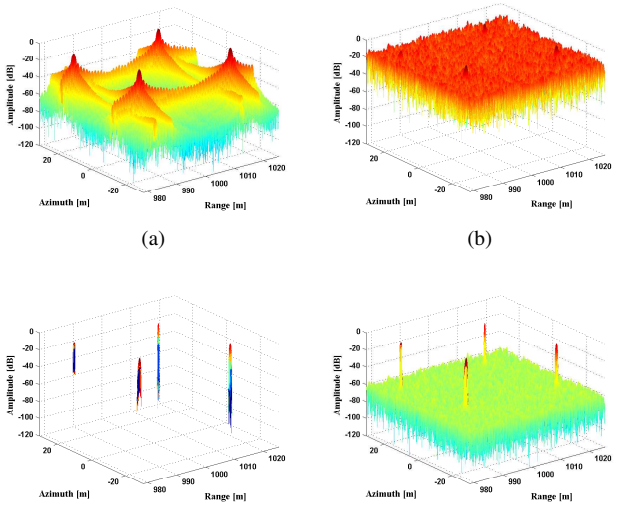

(a) (b)

(c) (d)

Fig. 2. Normalized results based on the simulated data with clutter by different methods. (a) Simulated scene, (b) MF, (c) sparse image $\hat{\mathbf{X}}_{SP}$ reconstructed by our proposed method, and (d) non-sparse image $\tilde{\mathbf{X}}_{SP}$ reconstructed by our proposed method.

TABLE II. TARGET-TO-BACKGROUND RATIO OF IMAGE RECONSTRUCTED BY MF AND THE PROPOSED METHODS.

Target	Target1	Target2	Target3	Target4
MF	22.57 dB	21.54 dB	21.04 dB	21.09 dB
Proposed Method	75.86 dB	65.08 dB	68.95 dB	64.46 dB

using the proposed method. Similar to Fig. 1(c), it not only finds four point targets accurately, but also keeps the clutter distribution. In other words, $\tilde{\mathbf{X}}_{SP}$ can be considered as the result obtained by decreasing the power of clutter for MF-based image.

B. TerraSAR-X complex image data

TerraSAR-X spotlight complex image data with 1 m resolution was used to further demonstrate the validity of our proposed method. The surveillance region is Qingdao, China with several scene types, *e.g.* sea surface, harbor, and urban.

Let N_{dt} and N_{all_target} denote the number of detected and all target pixels, respectively; N_{df} and $N_{all\_clutter}$ represent the number of detected false alarm and clutter pixels, respectively. The target detection probability can be defined as

$$P_d \triangleq \frac{N_{dt}}{N_{all\_target}}, \tag{15}$$

and actual false alarm rate is given as

$$P_{fa} \triangleq \frac{N_{df}}{N_{all\_clutter}}. \tag{16}$$

Since the proposed method can suppress sidelobes and clutter, it will increase the contrast between the ship and background (sea surface), and provide the target more obviously in the non-sparse reconstructed image, *i.e.*, it improves CFAR detection probability for small ships submerged in strong clutter (the backscatter coefficient of target only slightly higher than clutter) over MF-based imaging.

We chosen one area in TerraSAR-X image data only includes sea surface without any ship (see Fig. 3(a)). To illustrate the effectiveness of the proposed methods, we introduced several targets (Fig. 3(b)) with different size, amplitude, and phase to this area. Fig. 3(c) and Fig. 3(d) show CFAR detection results for MF-based image and non-sparse image based on our proposed method reconstruction with $P_{fa} = 10^{-5}$. CFAR can detect strong and large targets in both MF and CAMP-IM reconstruction images (indicated in the red rectangles), whereas small or weak targets, with similar amplitudes as surrounding clutter, cannot be detected in MF-based SAR images, but can be detected well in the non-sparse image (the cyan rectangle in Fig. 3(d)). To evaluate the performance of non-sparse image reconstruction by the proposed method for CFAR detection comprehensively. Let the image, a combination of Fig. 3(a) and Fig. 3(b), as the simulated scene, we perform the CFAR detection for the MF-based reconstructed result and our proposed method-based non-sparse image under different false alarm rate P_{fa}. The $P_d - P_{fa}$ curves for CFAR detection is shown in Fig. 4. For fixed P_{fa}, we can see that the detection probability in the non-sparse image is higher than MF, *i.e.* the non-sparse image reconstructed by our proposed method outperforms MF-based result in CFAR detection.

V. CONCLUSION

In this paper, we proposed a CAMP-based SAR image regularization reconstruction mechanism using complex image data. Compared to MF-based SAR image, our proposed method provide improved image performance, *e.g.*, significant sidelobe and clutter suppression. Furthermore, compared to other algorithms for solving the L_1 regularization problem, the proposed CAMP based algorithms provide the sparse image of the considered scene as well as a non-sparse estimation with similar background statistical properties to MF-based reconstructed images. An adaptive CFAR detector based on the non-sparse image reconstructed by the proposed method was

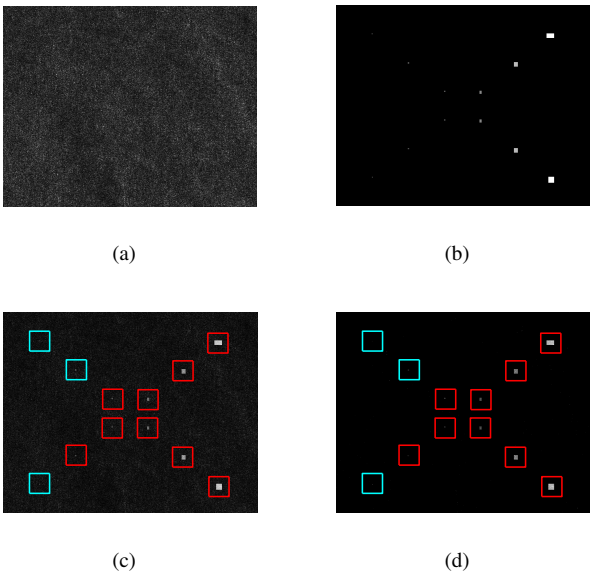

Fig. 3. CFAR detection of simulated targets on the sea. (a) Chosen sea surface in TerraSAR-X image. (b) Targets with different size, amplitude, and phase. (c) CFAR detection for MF-based image. (d) CFAR detection for non-sparse image reconstructed by the proposed method. Red = targets detected both in MF and non-sparse images. Cyan= targets only detected in the proposed method-based non-sparse image.

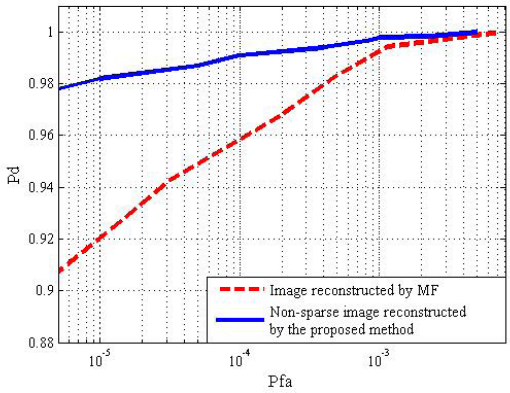

Fig. 4. $P_d - P_{fa}$ curves for CFAR detection based on the MF-based image and non-sparse image recovered by the proposed method.

designed and successfully employed for target detection on real TerraSAR-X complex image data. The non-sparse image reconstructed by the proposed method has better detection ability for weak target and higher detection probability with a fixed false alarm rate than MF-based SAR imaging.

ACKNOWLEDGMENT

This work was supported by the Chinese Academy of Sciences/State Administration of Foreign Experts Affairs (CAS/SAFEA) International Partnership Program for Creative Research Team, the National Natural Science Foundation of China under Grant 61571419 and 61471019. The authors would like to thank Prof. Jinping Sun with Beijing University of Aeronautics and Astronautics for providing the TerraSAR-X complex image data.

REFERENCES

[1] J. C. Curlander and R. N. Mcdonough, "Synthetic aperture radar: system and signal processing." New York, NY, USA: Wiley, 1991.

[2] F. M. Henderson and A. J. Lewis, "Principle and application of imaging radar." New York, NY, USA: John Wiley and Sons, 1998.

[3] I. G. Cumming and F. H. Wong, "Digital processing of synthetic aperture radar data: algorithms and implementation." Norwood, MA, USA: Artech House, 2004

[4] R. Bamler, "A comparsion of range-doppler and wavenamber domain SAR focusing algorithms," *IEEE Trans. Geosci. Remote Sens*., vol. 30, no. 4, pp. 706-713, Jul. 1992.

[5] R. K. Raney, H. Runge, R. Bamler, I. G. Cumming, and F. H. Wong, "Precision SAR processing using chirp scaling," *IEEE Trans. Geosci. Remote Sens*., vol. 32, no. 4, pp. 786-799, Jul. 1994.

[6] D. L. Donoho, "Compressed sensing," *IEEE Trans. Inf. Theory*., vol. 52, no. 4, pp. 1289-1306, Apr. 2006.

[7] E. T. Candès and T. Tao, "Near-optimal signal recovery from random projections: Universal encoding strategies," *IEEE Trans. Inf. Theory*, vol. 52, no. 12, pp. 5406-5425, 2006.

[8] R. Baraniuk and P. Steeghs, "Compressive radar imaging," in *Proc. IEEE Radar Conference*, Boston, MA, 2007. pp. 128-133.

[9] X. X. Zhu and R. Bamler, "Tomographic SAR inversion by L_1-norm regularization-the compressive sensing approach," *IEEE Trans. Geosci. Remote Sens*., vol. 48, no. 10, pp. 3835-3846, 2010.

[10] X. X. Zhu and R. Bamler, "Super–resolving SAR Tomography for Multidimensional Imaging of Urban Areas: Compressive sensing-based TomoSAR inversion," *IEEE Signal Processing Magazine*., vol. 31, no. 4, pp. 51-58, 2014.

[11] L. Zhang, M. Xing, C. Qiu, J. Li, and Z. Bao, "Achieving higher resolution ISAR imaging with limited pulses via compressed sampling," *IEEE Geosci. Remote Sens. Lett*., vol. 6, no. 3, pp. 567-571, 2009.

[12] A. C. Gurbuz, J. McClellan, and W. Scott, "A compressive sensing data acquisition and imaging method for stpped frequency GPRs," *IEEE Trans. Signal process*., vol. 57, no. 7, pp. 2640-2650, 2009.

[13] Y. Yu, A. Petropulu, and H. Poor, "MIMO radar using compressive sampling array processing," *IEEE J. Sel. Topics Signal Process*., vol. 4, no. 1, pp. 146-163, 2010.

[14] B. Zhang, W. Hong, and Y. Wu, "Sparse microwave imagingPrinciples and applications," *Sci. China Inf. Sci*., vol. 55, no. 8, pp. 1-33, 2012.

[15] D. L. Donoho, A. Maleki, and A. Montanari, "Message passing algorithms for compressed sensing," *Proc. Nat. Acad. Sci*., vol. 106, no. 45, pp. 18914-18919, 2009.

[16] A. Maleki, L. Anitori, Y. Zai, and R. Baraniuk, "Asymptotic analysis of complex LASSO via complex approximate message passing (CAMP)," *IEEE Trans. Inf. Theory*, vol. 59, no. 7, pp. 4290-4308, 2013.

[17] L. Anitori, A. Maleki, M. Otten, R. Baraniuk, and P. Hoogeboom "Design and Analysis of Compressed Sensing Radar Detectors," *IEEE Trans. Signal process*, vol. 61, no. 4, pp. 813-827, 2013.

[18] I. Daubechies, M. Defriese M, and C. De Mol, "An iterative thresholding algorithm for linear inverse problems with a sparsity constraint," *Commun. Pure Appl. Math*., vol. LVII, pp.1413-1457, 2004.

[19] S. Brusch, S. Lehner, T. Fritz, M. Soccorsi, A.Soloviev, and B. Schie, "Ship surveillance with TerraSAR-X," *IEEE Trans. Geosci. Remote Sens*., vol. 49, no. 3, pp. 1092-1103, 2011.

[20] M. Çetin, W. C. Karl, and D. A. Castanon, "Feature enhancement and ATR performance using nonquadratic optimization-based SAR imaging," *IEEE Trans. Aero. Elec. Sys*., vol. 39, no. 4, pp. 1375-1395, 2003.